HHS Public Access

Author manuscript

Dev Cell. Author manuscript; available in PMC 2019 May 07.

Published in final edited form as:

Dev Cell. 2018 May 07; 45(3): 316–330.e4. doi:10.1016/j.devcel.2018.04.007.

Mechanical strain determines cilia length, motility and planar position in the left-right organizer

Yuan-Hung Chien[1], **Shyam Srinivasan**[1,2], **Ray Keller**[3], and **Chris Kintner**[1,4]

[1]Molecular Neurobiology Laboratory, The Salk Institute for Biological Studies, La Jolla, CA 92037 USA

[2]Kavil Institute for Brain and Mind, University of California, San Diego, La Jolla, CA 92093 USA

[3]Department of Biology, University of Virginia, Charlottesville, VA 22904 USA

Summary

The *Xenopus* left-right organizer (LRO) breaks symmetry along the left-right axis of the early embryo by producing and sensing directed ciliary flow as a patterning cue. To carry out this process, the LRO contains different ciliated cell types that vary in cilia length, whether they are motile or sensory, and how they position their cilia along the anterior-posterior (A-P) planar axis. Here we show that these different cilia features are specified in the prospective LRO during gastrulation, based on anisotropic mechanical strain that is oriented along the A-P axis, and graded in levels along the medial-lateral axis. Strain instructs ciliated cell differentiation by acting on a mesodermal prepattern present at blastula stages, involving *foxj1.* We propose that differential strain is a graded, developmental cue, linking the establishment of an A-P planar axis to cilia length, motility, and planar location, during formation of the *Xenopus* LRO.

ETOC

The left-right body axis is established in *Xenopus* embryos by leftward fluid flow produced and sensed in the left-right organizer. Chien et al. show that the pattern of cilia differentiation required to produce this flow is determined by graded and oriented mechanical strain during gastrulation.

[4]Lead Contact: Kintner@salk.edu.

Declaration of Interests

The authors declare no competing interests

Author Contribution:

Conceptualization, Y.H.C. and C.K.; Methodology, Y.H.C. and C.K; Investigation, Y.H.C., R.K., and C.K; Writing Original Draft, C.K; Writing Review and Editing, Y.H.C. R.K. C.K. S.S.; Funding Acquisition, C.K.; Formal analysis, S.S.

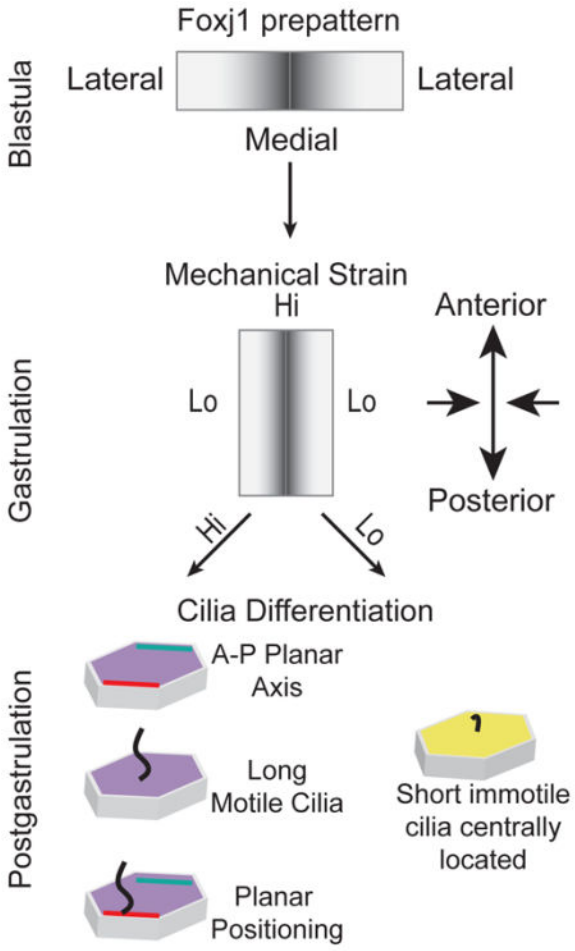

Introduction

Cilia are microtubule-based protrusions of the plasma membrane that vertebrate cells deploy to sense mechanical and chemical cues, and to generate directed fluid flow along luminal surfaces. This versatility is effectively exploited in the early vertebrate embryo within a structure called the left-right organizer (LRO), where ciliated cells produce and sense flow to break symmetry along the left-right body axis (Blum et al., 2014a; Hamada and Tam, 2014). Cilium differentiation in the LRO can vary based on length, structural features required for motility or mechanical sensing, and how a cilium is positioned within a cell in relation to the body axes. Here, we examine how these key ciliated features are specified during LRO formation in *Xenopus* embryos.

In *Xenopus,* the LRO epithelium is located at the posterior end of the gastrocoel roof plate (GRP), centered at the dorsal midline (Schweickert et al., 2007). As in the mouse, this epithelium is a relatively flat surface that can be divided along the medial-lateral (M-L) axis into domains containing ciliated cells with different specialized features (Boskovski et al., 2013; McGrath et al., 2003; Nonaka et al., 2005; Schweickert et al., 2010; Schweickert et al., 2007; Yoshiba et al., 2012). Cells located medially extend a single, relatively long motile

cilium (~8μm) required to be flow producers. Significantly, to generate a flow appropriately directed for L-R patterning, these cells also position their cilia along the anterior-posterior (A-P) planar axis of the apical domain towards the posterior cell edge, causing a posterior tilt and flow that moves from right-to-left (Okada et al., 2005; Schweickert et al., 2007). In contrast, cells located in lateral domains of the LRO extend relatively short (~4 μm) immotile cilia, required to be flow detectors (Yoshiba and Hamada, 2014). The cilia in these cells remain centrally located along the planar axis, a position perhaps more effective when detecting flow as a mechanical cue (Okada et al., 2005; Schweickert et al., 2007).

The mechanisms that specify cilium differentiation within LRO cells likely target foxj1, a forkhead transcription factor that plays a critical role in promoting motile cilium formation (Choksi et al., 2014; Stubbs et al., 2008). Loss of foxj1 in the *Xenopus* LRO not only leads to cilia shortening, and a loss of motility, but also a failure to properly position cilia posteriorly along the A-P planar axis (Campbell et al., 2016; Stubbs et al., 2008). *Foxj1* is already expressed at blastula stages, when the LRO anlage lies externally as a superficial epithelium wrapping the dorsal marginal zone, peaking in levels at the dorsal midline, where Spemann's organizer is located, and then grading off to lower levels more laterally (Blum et al., 2014b). Disrupting the early steps of axis formation alters the formation of Spemann's organizer and neighboring tissues, causing defects in the LRO and heterotaxy (Blum et al., 2014b). Various signaling pathways, including serotonin, Wnt, Notch, TGF-beta, and FGF, have all been shown to impact the length and/or formation of motile cilia in the *Xenopus* LRO, in some cases by influencing the early expression of *foxj1* (Beyer et al., 2012; Boskovski et al., 2013; Chu and Sokol, 2016; Neugebauer et al., 2009; Tozser et al., 2015; Walentek et al., 2012; Walentek et al., 2013). Thus, the formation of the LRO is intimately associated with early axial patterning of the marginal zone, leading to the idea that these early events specify the pattern of cilia differentiation that arises in the LRO after gastrulation is complete.

Cilia differentiation in the LRO is coordinated with the establishment of a planar axis that is used for cilia planar positioning, requiring the core planar cell polarity (PCP) pathway (also called Fz-PCP), whose conserved components act in numerous epithelia as a planar compass (Eaton and Julicher, 2011; Gray et al., 2011; Peng and Axelrod, 2012; Singh and Mlodzik, 2012). The core components of Fz-PCP, including three transmembrane proteins related to *Drosophila* Van Gogh (Vangl), Frizzled (Fzd) and Flamingo (Celsr), signal locally by direct cell-cell interactions, resulting in the formation of stable complexes of Vangl/Celsr and Fzd/Celsr that can overtly localize to opposing cell edges in a head-to-tail arrangement. In the LRO, the Fz-PCP components are polarized prior to cilia positioning (Hashimoto et al., 2010), with a vector directed along the A-P body axis: the anterior and posterior cell edges are the Vangl-enriched and Frizzled-enriched cell poles, respectively (Antic et al., 2010; Borovina et al., 2010; Chu et al., 2016; Hashimoto et al., 2010; Song et al., 2010). Current models suggest that medial LRO cells relocate the motile cilium, which initially forms at the geometric center, towards the posterior "Frizzled-enriched" pole, enabling the production of leftward flow. Formation of an A-P planar axis with the appropriate vector in the LRO is thought to involve additional global patterning cues that influence the orientation of Fz-PCP signaling when the planar axis first forms (Hashimoto and Hamada, 2010). A gradient of Wnt activity, for example, has recently been proposed to direct the formation of the AP

planar axis in the mouse LRO, based on a genetic analysis of posteriorly produced Wnt ligands, and anteriorly produced Wnt inhibitors (Minegishi et al., 2017). How the orientation of Fz-PCP signaling is influenced by these signals, and how direct their action, is still unclear.

The model that cilium differentiation in the *Xenopus* LRO is already patterned at blastula stages is difficult to reconcile with the fact that the LRO anlage undergoes a significant change in shape during gastrulation (Blum et al., 2014b; Shook et al., 2004). The LRO epithelium involutes into the embryo and deforms along the A-P axis (Fig. 1A–C) (Keller, 1975), presumably disrupting any spatial prepattern established earlier, but also generating additional mechanical cues that conceivably guide the formation of the LRO. Indeed, gastrulation movements are key for generating an A-P planar axis on the ventral side of the *Xenopus* embryo when the closing blastopore pulls the skin in a posterior direction (Chien et al., 2015). Since the LRO epithelium likely endures similar oriented strain during gastrulation, we considered the possibility that this strain is required to form an A-P planar axis needed for cilia positioning and leftward flow. To examine this possibility, we analyzed the pattern of strain that occurs in the LRO during gastrulation, and manipulated strain during LRO formation in both loss-and gain-of-function experiments. Results from these studies show that strain directs the formation of an A-P planar axis, but also specifies cilia differentiation along the M-L axis, acting as a determinate of cilium length, motility, and planar positioning during LRO formation.

Results

LRO cells incur relatively high rates of strain during gastrulation

The *Xenopus* fate map (Keller, 1975) was used to estimate strain levels at different positions in the gastrocoel roof plate (GRP) during gastrulation. Colored patches placed on the involuting marginal zone (IMZ, shaded gray area in Fig. 1A) are followed through the late midgastrula (Fig. 1B) to the end of gastrulation (Fig. 1C) to map the movements of the presumptive GRP (based on (Keller, 1975;1976), see Fig. S1A–B). The presumptive GRP begins its involution by rolling over the blastoporal lip (black arrows, in Fig. 1A) at the onset of gastrulation, and as it involutes, it shows postinvolution convergence and extension (CE, blue/green arrows, Fig. 1B,C), beginning in its dorsal (presumptive anterior) sectors and progressing toward the ventral side of the gastrula (presumptive posterior) sectors to form the GRP (visualized turned inside out in a cut-way of the dorsal presumptive neural and epidermal tissues, Fig. 1B). Continued, post-involution CE closes the blastopore and simultaneously elongates the GRP by the end of gastrulation (blue/green arrows, Fig. 1C). CE is expressed progressively in the IMZ, beginning dorsally (presumptive anterior) and progressing ventrally (presumptive posterior), and it is more extensive, from a minimum at the lower edge of the IMZ where it bounds the endoderm (light shading), to a maximum (dark shading) at the Limit of Involution (LI) (Fig. 1A–C) (Shih and Keller, 1992). The result is a progressive increase in CE dorsally and posteriorly in the GRP (dark shading, Fig. 1C). Because there is no significant growth or increase in cellular volume in the early *Xenopus* embryo (Tuft, 1962), and change in tissue thickness is fairly uniform to this stage, the narrowing and lengthening (CE) shown (Fig. 1C), approximates the total tissue strain in

the GRP. As a result, there is a fall-off of A-P strain on both sides of the midline everywhere along the A-P axis but especially posteriorly where the LRO will be located (see box, Fig. 1C) and also a progressive increase in strain from anterior-to-posterior due to the intercalation of more cells, and thus more CE, posteriorly (Keller and Jansa, 1992; Shih and Keller, 1992). In sum, the fate map predicts the developing LRO anlage is likely to endure significant levels of strain during gastrulation prior to ciliation, highest at the midline, and graded both along the M-L and A-P body axes.

LRO cells elongate in proportion to strain rates

We previously monitored several parameters as surrogates to gauge the levels of mechanical strain that occurs in ventral skin cells during gastrulation (Chien et al., 2015). Skin cells, for example, respond to strain by elongating, measured as a length-width ratio (LWR, cell length measured along the longest axis of the apical surface versus cell width along the orthogonal axis) (Chien et al., 2015). LRO cells are similarly elongated after gastrulation (stage 12), with the long axis aligning to the A-P body axis (Fig. S1C–E), with a magnitude significantly higher than that previously found in the ventral skin at the same stage (LWR: 2.78±1.2 versus 1.72±0.39, p=9XE-31, Fig. 1E, Table S1), and in a pattern that peaks at the dorsal midline (3.18±1.98, Table S1) and tapers to a lower value in lateral regions (1.98±0.68. Table S1) in a graded, near-linear manner (Fig. 1F, Fig. S1F, Table S1). At subsequent stages, when cilia form and position posteriorly, the elongation of LRO cells is markedly reduced (LWR=1.57±0.36, Fig. 1E), and not aligned to any particular axis (Fig. S1E). Thus, the orientation and magnitude of cell elongation indicates that LRO cells are subjected to A-P oriented strain graded along the M-L axis during gastrulation prior to ciliation.

LRO cells polarize apical microtubules differentially along the M-L axis

The ventral skin epithelium also responds to strain by forming a network of non-centrosomal microtubules (MTs) at the apical surface that can be visualized by tracking the directional movements of Clip170-GFP, a marker of plus-end MT assembly (Fig. S2A–B) (Chien et al., 2015). We previously used this assay to show that apical MTs are polarized in the ventral skin at stage 12, since 62±5% of the Clip170-GFP comets track parallel to the A-P planar axis (Table S1) (Chien et al., 2015). These polarized apical MTs are lost if the skin is explanted before gastrulation and cultured to a stage 12 equivalent (thus eliminating strain), but can be largely restored in these explants by applying exogenous strain. Exogeneous strain was applied to these and the explants described below by aspirating the tissue into a glass capillary for 3hrs (time of gastrulation), employing a specific level of negative pressure (Chien et al., 2015). In the previous study, skin explants were strained using a level of treatment resembling that occurring during gastrulation (resulting in a LWR of ~1.7 in responding cells). More recently, we found that when these explants are strained at even higher levels by aspiration (resulting in a LWR of ~2.3 on average), the fraction of Clip170-GFP comets aligned to the axis of strain in responding cells increased from 61±4.6% to 76±1% on average (Fig. S2C–D, p=0.0056; Table S1). Thus, the degree of apical MT alignment, like the levels of cell elongation (LWR), can be used to estimate strain levels.

When LRO cells were examined at stage 12 using the Clip170-GFP assay, we detected an apical MT network resembling that in the skin (Fig. 1G, Fig. S2A), but with an even greater fraction of the comets aligning preferentially to the A-P planar axis (76±4 vs 62±5%, p=0.019) (Table S1) (Chien et al., 2015). In addition, the fraction of Clip170-GFP comets aligned to the A-P planar axis was markedly higher in medial versus lateral LRO cells (86±6% versus 52±11%, p=0.011), consistent with a high to low pattern of strain (Figs. 1G–H and S2F–G, Table S1). We further compared the degree of apical MT alignment in LRO cells by calculating how the directed movement of individual Clip170-GFP comets deviated within a cell from the mean orientation (MTSD), using the approach described by Gomez et al (Gomez et al., 2016). While apical MT orientation in medial LRO cells deviated on average by 26±5.4 degrees from the mean, those in lateral LRO cells deviated 52±7.7 degrees (p=1XE-5, Figs. 1I, Table S1). Thus, the pattern of apical MT orientation/alignment in the LRO supports the view that a high to low pattern of A-P oriented strain occurs along the M-L axis of the LRO during gastrulation.

LRO cells polarize Fz-PCP components along the A-P planar axis

The ventral skin also responds to strain during gastrulation by forming an A-P planar axis that can be detected by measuring the stability of core PCP components using fluorescent recovery after photobleaching (FRAP) (Strutt et al., 2011). In this assay, GFP-tagged PCP components (fz3, celsr1, or vangl2) are expressed in embryos (using low levels that do not disrupt development), short junctional segments are subjected to FRAP, and the resulting plateau of recovery is used to estimate the fraction of PCP components existing in stable complexes (Chien et al., 2015). In the ventral skin, this assay detects a planar axis that arises after gastrulation, based on a marked increase in the stable fraction of Fz-PCP components that occurs selectively at junctions oriented orthogonal to the A-P axis (Chien et al., 2015). This assay also detects a similar planar axis in the LRO at stage 12 since PCP components (GFP-tagged fzd3 and celsr1) show a similar marked stable fraction at the junctions oriented orthogonal but not parallel to the A-P axis (Fig. S2H–I, Table S1). In the LRO, the average stable fraction that appears at orthogonal junctions is even higher than that previously observed in the skin, consistent with the idea that higher levels of strain promoting PCP signaling leads to an increase in stable complexes (52.3±9.1 vs 38.6±4.7%, p=0.001, Table S1) (Chien et al., 2015). Furthermore, the fraction of stable fzd3-GFP at orthogonal junctions was also higher in medial versus lateral LRO cells (51±5% vs 36±11%, p=0.008. Fig. 1j), as would be predicted if oriented strain occurs from high to low levels along the M-L axis of the LRO during gastrulation.

Strain patterns along the M-L axis correlate with cilia length and planar positioning

The results above indicate that strain is graded along the M-L axis of the LRO during gastrulation, potentially affecting how these cells undergo cilia differentiation. To examine this possibility further, we measured cilia length and planar positioning in LRO cells at stage 18, according to their M-L position (Fig. 1K, Fig. S3A). Cilia length shows a graded distribution with a peak at the dorsal midline of 9 μm on average falling to 4 μm on average within the lateral domain. Significantly, the distribution of cilia length is not bimodal, as one might predict if the LRO consisted of two distinct ciliated cell types, but rather falls along a continuum that varies in a near linear manner, mirroring the change in LWR along the M-L

axis at stage 12 (Fig. 1K vs Fig. 1F). We also plotted the planar position of cilia in LRO cells located at different points along the M-L axis (Fig. 1L, Fig. S3B). This plot shows that LRO cells at the dorsal midline position their cilia the furthest in a posterior planar direction, while those located in the lateral LRO remain in a more central planar position, with a graded planar positioning in between. Thus, graded strain along the M-L axis of the LRO during gastrulation prefigures a graded pattern of cilium length and planar positioning that appears later. In addition, these data indicate that cilia subtypes in the LRO do not fall neatly into two distinct groups, but have graded properties, at least in terms of cilium length and planar positioning.

Dorsal explants, lacking strain, have defects both in cilium formation and planar positioning

To assess the role of strain in patterning cilium differentiation in the LRO, we employed explants that disable gastrulation-mediated axial elongation. In one approach, the entire dorsal marginal zone (Fig. 2A), along with the adjacent dorsal ectoderm, was explanted from blastula stage embryos, and placed onto a glass coverslip coated with high concentrations of fibronectin (FN), with the deep cells down (Fig. 2B, referred to hereafter as FN explants). Davidson et al (2004) showed that axial extension largely fails in FN explants because the deep mesodermal cells adhere too tightly to the fibronectin substrate to converge and extend (Fig. 2C). Despite the failure to elongate, however, notochord and somite differentiation within FN explants is preserved, but occurs according to their position in the blastula fate-map, indicating that many of the signals required for tissue differentiation remain intact (Davidson et al., 2004).

The average LWR of the LRO cells in FN explants at a stage 12 equivalent was markedly less than that of LRO cells *in situ* (1.7±0.4 versus 2.7±1.1, p=3.9XE-23), consistent with a reduction in strain upon explantation (Fig. 2F, FN, versus Fig. 1E, Table S1). We further scored cilium planar positioning in LRO cells in FN explants (at a stage 18-equivalent) by expressing cep152-GFP to mark the basal body. Cilia within the LRO cells at this stage *in situ* are largely located towards the posterior cell edge (Fig. 2G), but those in FN explants largely remained located in a central planar domain (Fig. 2H, Table S1). Finally, we scored cilia length in FN explants and found that they were significantly shorter than that normally present in the LRO (4.15±2.04 vs 8.34±1.72 μm, p=3.6XE-06) (Fig. 2J, FN versus LRO, Table S1). Thus, cilia differentiation, both in terms of planar positioning and cilium length, is compromised when axial elongation in the LRO is reduced.

The ciliation defects in the FN explants could be due to the fact the mesoderm fails to involute as normally occurs during gastrulation (Fig. 1A–C), thus disrupting interactions with the overlying neural tissue, and exposing the LRO to an external environment. To address this concern, we combined two dorsal sides into a Keller sandwich (KS explants) (Fig. 2D) (Keller, 2012) where axial extension but not involution now occurs, resulting in an inside-out configuration where the LRO extends away from the neuroectoderm (Fig. 2E). Axial elongation in a KS explant drives cell elongation (LWR=2.5±0.8) in the LRO to a similar degree as in embryos (Fig. 2F, KS versus Fig. 1E, st12, Table S1). Cilia in the LRO cells of a KS explant (at a stage18 equivalent) resembled those in a wildtype embryo, both in

terms of their average length (7.34±2.23μm, Fig. 2J, Table S1) and their ability to position along the A-P planar axis of the apical surface (Fig. 2I vs 2G, Table S1). Thus, the superficial mesoderm within the LRO need not involute to form the long, polarized cilia normally found within the central region of the LRO.

The planar axis fails to form in explanted LRO tissue but can be rescued and aligned using exogenously applied strain

Restoring strain to a FN explant is challenging, leading us to employ a different LRO explant more amenable to strain manipulation. This explant was generated by dissecting the superficial epithelium located at the dorsal midline of the marginal zone of blastula-stage embryos (stage 10.5), containing the prospective medial LRO (Fig. 3A), along with the attached deep mesodermal cells (referred to hereafter as a LRO explant). When placed in culture, the superficial LRO anlagen in these explants encapsulates the deep cells within 30 minutes to form a tissue ball (Fig. 3B), and remains on the surface. The deep cells are unable to effectively undergo their normal gastrulation movements, resulting in variable but little elongation over the next 4–8 hours. As a consequence, the LRO anlage incur little strain in LRO explants: the LWR of the LRO cells in these explants at a stage 12 equivalent was markedly reduced from normal (1.56±0.33, Fig. 3D, Table S1) and the long axis of these cells failed to consistently align to any particular axis (Fig. 3E). Strain was then restored by aspirating these explants for three hours (the time of gastrulation) into a small-bore glass capillary using a precise level of negative pressure (Fig. 3C)(Chien et al., 2015). We empirically determined conditions (216μm capillary diameter and 50 Pa of pressure) where the LRO epithelial cells in strained explants elongated to an average LWR of 2.7±1.1 after 3 hrs of aspiration (Fig. 3D versus Fig. 1E), in line with the LWR of LRO cells *in vivo* after gastrulation (p=0.4, Table S1). Thus, this approach consistently reduces and then restores physiological-relevant levels of strain to the LRO anlage over the relevant developmental time period.

We first examined the status of the planar axis in unstrained and strained LRO explants, since strain is required for an planar axis to form in the ventral skin (Chien et al., 2015). In unstrained LRO explants, we failed to detect junctions with an increased stable fraction of GFP-tagged fzd3, celsr1 or vangl2 (Fig. 3G–I, No strain) at a stage12 equivalent, even though at this stage, such junctions were readily detected in the LRO (Figs. 1J, S2H,I). In contrast, the stable fraction of all three GFP components markedly increased in the LRO explants treated with aspiration, but only at those junctions positioned orthogonal to the axis of strain application (Fig. 3G–I, Table S1). The formation of an A-P planar axis in the LRO, therefore, also appears to be strain dependent.

Motile cilia formation and polarization fails in LRO explants, but can be rescued by exogenous strain

We further analyzed strained or unstrained LRO explants, by scoring cilia length and motility, at a stage 18-equivalent (Fig. 4A–B). Cilia that formed in unstrained explants were extremely short (1.6±0.4μm, Fig. 4A,C) compared to the average cilia length in the LRO *in situ* (8.34±1.72 μm, Fig. 2J). When these cilia were labeled using Arl13b-GFP, and imaged using high-speed confocal microscopy to score motility (Boskovski et al., 2013), very few

cilia forming in unstrained LRO explants appeared to move (6/60 motile cilia scored in 4 explants, Movie S1). We also scored motile cilia differentiation by expressing a GFP-tagged form of tektin2, a gene previously found to be markedly upregulated by foxj1 (Stubbs et al., 2008). Tetkin2-GFP localizes to the axoneme in most medial but few lateral LRO cells (Table S1) and this localization is lost in medial cells in *foxj1* mutants (Fig. S4), as motile cilia are lost (Stubbs et al., 2008). Tektin2-GFP also did not strongly localize to the cilia in unstrained LRO explants consistent with a lack of motile character (Fig. 4D, Table S1). In contrast, in LRO explants strained by aspiration, cilia length at a stage 18 equivalent was statistically indistinguishable from that forming on medial LRO cells (7.96±2.83 vs 8.34±1.72 μm, p=0.3, Table S1) (Fig. 4B,C vs Fig. 1, 2J), most of these cilia appeared motile when these explants were live imaged in the same way as the unstrained explants (54/58 motile cilia scored in 4 explants; Movie S2), and tektin2-GFP localized to their axenome (Fig. 4E, Table S1). Cilium differentiation in LRO explants, therefore, resembles that of lateral LRO cells in the absence of strain, and that of medial LRO cells following treatment with exogenous strain.

Cilia length is a function of strain levels

Since the change in cilium length in LRO explants in response to aspiration was unexpected, we explored whether this response was dependent on strain levels or duration, rather than the fact the LRO epithelial cells were simply positioned inside a capillary tube during aspiration. When LRO explants were aspirated into glass capillaries as above, but using less negative pressure (20Pa versus 50Pa) to reduce strain levels, but with the same duration (3hrs), explants formed cilia that were longer on average than those in unstrained explants (3.48±1.87 versus 1.60±0.4 μm, p=4XE-25), but considerably shorter than those in explants treated with greater strain (Fig. 4C; Table S1). Since explants in both cases were deformed geometrically in a similar way, but differed mainly in strain levels, this observation suggests that the latter was critical in specifying cilium length.

We tested strain duration by aspirating LRO explants into the capillary for one hour, equalizing the pressure to reduce further strain, while leaving the explant in the capillary for an additional two hours, before expelling (Fig. 4F). As a control, the LRO explants were strained for the full 3 hrs, before expelling (Fig. 4F). When cilium length was measured in both explants, in just the 200μm tip (Fig. 4F), the cilia in explants strained for just one hour were considerably shorten on average than those strained for entire 3 hours (4.06±1.89μm versus 8.78±2.98μm, p=3XE-28), even though the strain levels used (when applied) were comparable (Fig. 4G). This result supports the model that the duration of strain application, along with strain levels, is a key factor in promoting cilia lengthening.

We also scored cilium length in LRO explants aspirated for 3 hrs at 50Pa, as a function of their position within the explants. Explants move into the capillary at a constant rate during aspiration (data not shown), indicating that strain duration is likely to vary along the explant in a linear manner. Once explants are expelled after strain treatment, they round backup to some degree, but remain oblong, allowing one to relate cilium length to strain duration: cells entered the capillary first (longest strain exposure) versus last (shortest strain exposure). This plot shows that cilium length varies according to cell position (Fig. 4H), indicating a near

linear relationship between the duration of strain application and the response in terms of cilium length. This relationship closely resembles that between cilium length and cell location along the M-L axis of the LRO (Fig. 1K). Together these results indicate that cilium length in LRO explants is mainly a function of strain (both levels and duration), suggesting strongly that the two are functionally connected.

Planar positioning of cilia following strain

We next examined the planar location of cilia in unstrained and strained LRO explant cells at a stage-18 equivalent, by marking the basal body with cep152-GFP and confocal imaging the apical surface (Fig. 4A). In unstrained explants, cilia remained located within the central domain of the cell's apical surface (Fig. 5B), and there was little coordination of planar positioning locally (Fig. 5D), thus resembling the pattern of cilia positioning in lateral LRO cells at stage 18 (Fig. 5G, Table S1). This result was expected since these explants lack a planar axis, based on the FRAP analysis, and their cilia short and immotile. Since a planar axis and long motile cell differentiation can be rescued in LRO explants by strain, one would predict that the two conditions required for planar positioning are now met. Indeed, in strained LRO explants examined at stage 18, cilia were now positioned outside the central apical domain (Fig. 5C), thus closer to the cell edge, measured either along a normalized radius, or by absolute distance from the geometric center (Table S1). Strikingly, this planar positioning did not occur randomly, but rather coordinately between cells locally (Fig. 5E), along an axis defined by the axis of strain (Fig. 5C, inside to outside), thus repositioning in same direction: e.g. towards the cell edge closest to the opening of the capillary during strain (Fig. 5C, Outside). Indeed, the degree of cilia planar polarization induced in LRO explants by aspiration closely resembled that normally found in the medial LRO cells *in situ* at stage 18 (Fig. 5C versus 5H. Table S1).

The implication of this result is that LRO explants respond to strain by not only forming a Fz-PCP axis as shown above, but also a consistent PCP vector, where the Frizzled pole is positioned towards the cell edge closest to the capillary opening during strain application. The analysis of apical MTs, using the clip170-GFP assay described above, already provided a hint that a consistent planar vector arises following strain. In the LRO, the direction of plus-end assembly of apical MTs is biased towards the posterior pole (Fig. 1G, 44±4% directed posteriorly versus 32±4% directed anteriorly, p=0.008). Furthermore, skin explants treated with a relatively high level of exogenous strain responding by forming MTs with a similar bias in the direction of plus-end assembly, in this case, towards the cell edge located closest to the capillary opening during strain (Fig. S2C,E, 46±7% directed outside versus 30±7% directed inside, p=0.004). Such biases in the direction of plus-end apical MTs in *Drosophila* have been proposed to influence the vector of Fz-PCP signaling, by enabling vesicular bound Frizzled and Dishevelled to traffic from one side of the cell to the other in a directional manner, when a planar axis forms (Harumoto et al., 2010; Matis et al., 2014; Shimada et al., 2006). Thus, apical MTs in the LRO or induced by strain consistently bias their plus-ends towards a cell edge that would be predicted to be the "Frizzled pole".

To test this prediction, we generated LRO explants that express fzd3-GFP in isolated cells by injecting just one side of the two-cell embryo with *fzd3-GFP* RNA. As LRO explants made

from these embryos are strained, cells intercalate and isolated fzd3-GFP expressing cells arise that can be used for FRAP analysis of opposing junctions in the same cell. In these cells, the stable fraction of fzd3-GFP was markedly higher at the orthogonal cell edge located closest to the capillary opening versus the opposing cell edge (58.66±9.52% versus 9.11±7.32%, p=3.2E-07) (Fig. 5I; Table S1), supporting the interpretation that strain is sufficient to generate a PCP vector required for cilia repositioning.

The role of a prepattern in the strain response

We next asked how the strain response of LRO explants observed above relates to the idea that the LRO anlage is already patterned at the blastula stages, prior to gastrulation. To examine this relationship, we carried out strain experiments on explants of the marginal zone located further from the dorsal midline, centered at 45 degrees or 90 degrees around the circumference (Fig. 5J and N). Left unstrained, the epithelial cells in both these explants formed short cilia (Fig. 5M,Q vs Fig. 4C) that remained in a central planar position, resembling the cilia features in unstrained LRO explants (Fig. 5K,O versus Fig. 5B). While essentially all cells in the 45 degrees explants formed cilia, only about a third of the cells in 90 degrees explant did so. When these two explants were subjected to aspiration using the same conditions used for LRO explants, they also responded by forming significantly longer cilia but in a graded manner: LRO explants (7.96±2.83 μm) were the longest, 45 degree explants intermediate (5.74±2.67μm, p=7.8XE-9), and 90 degree explants the shortest (3.61±1.99μm, p=2.4XE-33) (Fig. 5M,Q vs Fig. 4C). Significantly, 90 degree explants not only responded to strain by forming longer cilia, but also by increasing the percentage of cells that were ciliated (86.5%versus 32.5%). Finally, the cilia that formed in 45 and 90 degree explants showed less planar positioning compared to LRO explants (Fig. 5L,P vs C), although some directed planar positioning still occurred in the 45 degree explants (Fig. 5L). Together these results indicate that strain, as a factor promoting longer cilia and planar positioning, is instructive to cells in both the medial and lateral LRO anlage while a prepattern along the dorsal-ventral axis of the blastulae marginal zone influences the response to strain.

The role of foxj1 in the strain response

The results above indicate strain acts on a prepattern in the LRO anlage to link the formation of long motile cilia to planar repositioning. This link is already evident in *foxj1* mutants since both motile cilia differentiation and their planar positioning are coordinately disrupted (Campbell et al., 2016). We therefore asked if a similar linkage is seen when LRO explants are subjected to strain and mutant for foxj1.

We generated *Xenopus* embryos lacking foxj1 activity by injecting a previously described *foxj1* gRNA along with Cas9 protein at the one-cell stage (Campbell et al., 2016). Cilia length and planar positioning was first assessed in the LRO of these embryos at stage 18, but separately in medial and lateral cells. Average cilium length in medial LRO cells was markedly shorter in *foxj1* mutants, similar to that of wildtype lateral LRO cells (3.35±1.32μm versus 4.96±1.28μm, Fig. 6D, Table S). Moreover, cilia planar positioning was also markedly disrupted in the LRO of *f*oxj1 mutants, in that medial LRO cells failed to position their cilia towards the posterior pole (Fig. 6C). Interestingly, the planar positioning

of cilia within the medial LRO cells in *foxj1* mutants were more dispersed than those in lateral LRO cells (Fig. 6C versus Fig. 6B), perhaps due to the higher levels of strain that occur medially versus laterally during gastrulation as shown above. We examined this possibility by making LRO explants from *foxj1* mutants, and subjecting them to strain using aspiration using the same conditions described above (Fig. 6E). In contrast to wildtype LRO explants, *foxj1* mutant LRO explants failed to respond to strain by increasing cilia length (Fig. 6H, Table S1), or by positioning their cilia along a planar axis (Fig. 6G vs Fig. 5C, Table S1). We confirmed that *foxJ1* mutant LRO explants still formed a planar axis in response to strain (Fig. S5A, Table S1). Finally, we found that cilia dispersed more along the planar axis in *foxj1* mutant LRO explants subjected to strain compared to those left unstrained (Fig. 6G versus 6F, Table S1), mirroring the difference between medial and lateral LRO cells in *foxj1* mutants (Fig. 6C versus 6B). These observations indicate that: (1) foxj1 is required for motile cilia formation and planar positioning in response to strain, (2) foxj1 is not required for a planar axis to form in response to strain, and (3) cilia planar positioning in the lateral LRO is not only explained by the lack of motile cilia but also by the relatively low levels of strain that occur in this region during gastrulation.

Foxj1 is not sufficient to respond to strain

The results obtained above led us to ask whether foxj1 is sufficient to respond to strain in terms of cilia lengthening and planar positioning. To address this issue, we exploited the fact that, the superficial epithelium in the developing skin never becomes ciliated, but will respond to *foxj1* RNA injection by forming ectopic, LRO-like, motile cilia (Stubbs et al., 2008). These ectopic cilia reach ~5μm in length on average in the skin by stage 19 (Fig. S5B) but failed to polarize along a planar axis (Fig. S5C, Table S1). Since strain levels during gastrulation are markedly less in the skin versus LRO, we asked whether applying exogenous strain to skin explants expressing Foxj1 would result in longer cilia or planar positioning (Fig. 7A). Cilia in these explants did not detectably change in length in response to strain (Fig. 7D, Table S1) and remained tightly clustered within the geometric middle, showing little repositioning along a common planar axis (Fig. 7B,C, Table S1). Thus, the response to strain in the LRO explants were not recapitulated in the ectodermal explants, even though these explants have a robust A-P planar axis and motile cilia.

Cilia lengthening and polarization in mesoderm induced by Nr2

To determine whether cilia differentiation in response to strain is a specialized feature of embryonic mesoderm,, we converted the ectodermal explants used above into marginal zone mesoderm, by injected embryos at the two-cell stage with RNA encoding the mesodermal inducer, nodal-related 2 (nr2) (Schier, 2003). We first examined these nr2 explants to assess whether they indeed changed cell fate from ectoderm to mesoderm. First, nr2 explants failed to form multiciliated cells or ionocytes based on marker staining (data not shown), two of the prominent cell types associated with ectodermal lineages (Stubbs et al., 2008; Quigley et al., 2011). Second, RNAseq analysis was carried out on nr2 explants at a stage-14 equivalent, and compared to a previous RNAseq analysis that was performed on ectodermal explants at a similar stage as a control (Quigley and Kintner, 2017). Nr2 explants prominently upregulated genes associated with the fate of the lateral marginal zone mesoderm (e.g. muscle differentiation), including muscle transcription factors, segmentation

genes, as well as markers of the lateral LRO, dand5 and nr1 (Table S3, Fig S6) (Blum et al., 2014b). By contrast, ectodermal explants prominently upregulated genes associated with multiciliated cells and ionocytes, and with ectodermal progenitors (tp63, grhl1, tfap2c) (Table S3, Fig. S6) (Quigley and Kintner, 2017). Finally, while the superficial epithelium in ectodermal explants is never ciliated, the epithelium in nr2 explants extended short, largely immotile cilia (1.74±0.53μm, 27/86 motile cilia in 4 explants, Fig. 7H), resembling those that form on the unstrained medial and lateral LRO explants (Table S1). In sum, we conclude that expression of *nr2* is sufficient to convert ectoderm into marginal zone mesoderm.

The superficial epithelium in nr2 explants prepared from these embryos (referred to hereafter as nr2 explants) also failed to elongate based on LWR analysis, indicating they lacked strain (Fig. S5D,F). We treated nr2 explants with strain by aspiration, using the same conditions employed with the LRO explants, resulting in similar levels of strain based on the LWR measurements (Fig. S5E,F). Nr2 explants responded to strain by forming longer cilia (Fig. 7H, Table S1), in a duration-dependent manner (Fig. S5G), that were motile (78/82 motile cilia in 4 explants), thus resembling the response of the LRO explants. These data support the view that cilia differentiation in response to strain occurs in an embryonic mesodermal context.

Strain response in nr2 and foxj1 expressing explants

The cilia in nr2 explants following strain were not as long as those in LRO explants (6.39±2.62μm versus 8.34±1μm, p=9XE-6 Fig. 7H) and moreover failed to reposition along a common planar axis. We reasoned that nr2 explants may resemble the lateral LRO anlage, consistent with the finding that cilia length and positioning in response to strain in this tissue is not as robust as the medial LRO anlage (Fig. 5M versus Fig. 4C). In addition, since *foxj1* is already expressed in a prepattern along the M-L axis of the LRO anlage, we reasoned that foxj1, required for a robust response, is conceivably limiting in nr2 explants. To test this possibility, we generated ectodermal explants expressing both foxj1 and nr2, and subjected these explants to exogenous strain (Fig. 7I). *Foxj1/nr2* explants responded to strain by forming longer cilia, approaching a length and distribution indistinguishable from that observed in the LRO (8.32±2.44μm versus 8.34±1μm, p=0.95, Fig. 7L; 15), and by positioning their cilia along the planar axis, towards the side closest to the opening of the capillary, as observed in LRO explants (Fig. 7K). Thus, these experiments deconstruct the critical developmental steps required for LRO formation, beginning with the formation of a competent epithelium during mesodermal induction and patterning, followed by the specification of cilia differentiation in this epithelium by a gradient of mechanical strain during gastrulation (Fig. S7).

Discussion

Our results support a model where mechanical strain during gastrulation is a multifaceted cue that coordinately directs several significant ciliated features of the LRO. Strain is oriented along the A-P body axis, promoting Fz-PCP signaling and the formation of an A-P planar axis required for the cilia positioning and the generation of leftward flow. Strain

levels are graded along the M-L axis, acting as an instructive graded cue to influence cilia length, planar positioning, and then a switch from immotile to motile subtype as the LRO forms. We show that strain acts on a prepattern, involving foxj1, which is likely to be established in the dorsal marginal zone of the blastula during mesodermal induction. Our model emphasizes a complex interplay between a prepattern established during mesodermal induction, and mechanical forces occurring during gastrulation, to produce the A-P planar axis and differentiated ciliated cell types required for L-R patterning (Fig. S7).

Strain promotes the formation of an A-P planar axis in the LRO

Our findings show that strain produced by gastrulation acts on the LRO epithelium as a global cue to promote and align Fz-PCP signaling to the A-P body axis. This finding mirrors similar observations in the ventral skin, and indicates more generally that mechanical forces produced by gastrulation instruct the formation of an A-P planar axis in different germ layers in *Xenopus* embryos (Chien et al., 2015). In the LRO, however, strain produced by gastrulation is even more pronounced than that occurring ventrally, promoting even greater cell elongation, sharper orientation of apical MTs, and even higher levels of stable PCP components, presumably as a downstream consequence. These results emphasize that strain can ensure that Fz-PCP signaling is globally coordinately, and that the Fz-PCP axis forms rapidly. Both factors are likely to be important, given the small window of developmental time devoted to cilia formation, polarization and function within the *Xenopus* LRO.

We also find that strain applied to LRO explants is sufficient to induce a consistent PCP vector, allowing cells to position the Fzd3 pole in the same planar direction, and their cilia towards this pole. How global cues determine the direction a planar vector remains poorly understood, but can be influenced by prepatterns such as the Fat/Daschous/Four-jointed pathway in *Drosophila* or by secreted Wnt ligands (Matis et al., 2014; Shimada et al., 2006) (Minegishi et al., 2017). In our experiments, however, foxj1/nr2 explants repositioned their cilia along the same planar axis following strain treatment, and skin explants consistently biased their plus-end MT assembly along the same planar vector following exposure to high strain. Since it is difficult to imagine how these explants acquired a consistent prepattern, our results would seem to argue against a pre-existing bias, but rather for a model where a PCP vector is specified during strain application. One possibility is that this specification depends on the fact that strain both in the LRO *in situ* and during aspiration occurs in a temporally and spatially graded manner.

Foxj1 is required but unlikely to be sufficient to respond to strain

Our findings show that strain levels varies in a graded manner along the M-L axis of the LRO during gastrulation, and that this graded cue is sufficient to produce a graded pattern of cilia length/planar positioning, and a shift from immotile to motile cilia as the LRO forms and functions after gastrulation. We favor the model that graded signals occur in the LRO in response to different strain levels and durations, since such signaling has been shown to occur when epithelial cells relieve the stress that strain inflicts, for example by remodeling apical junctions, and/or by breaking and making new basal contacts with the underlying matrix/mesenchymal cells (reviewed in (LeGoff and Lecuit, 2015)). The simplest model is that strain acts on *foxj1* expression, since foxj1 is required for motile cilia formation in the

LRO, and to respond to strain. Moreover, *foxj1* expression has been shown to increase in a kidney disease model in response to tubule dilation where strain likely occurs (Hellman et al., 2010). However, we have detected only a small increase in *foxj1* expression (Fold-change=1.58±−0.2) in strained versus unstrained LRO explants using quantitative PCR. In addition, while expression of high levels of *foxj1* by RNA injection can increase cilia length in the LRO, nr2 and skin explants to some extent, strain is still required to the reach the peak lengths seen at the midline of the LRO *in situ*. Thus, we suggest that while foxj1 is absolutely required for motile cilia differentiation in the LRO, strain likely act via additional pathways, either by modulating foxj1 activity post-transcriptionally, or by acting via unknown modulators of cilia differentiation.

Strain response depends on a mesodermal prepattern involving foxj1

Previous studies have shown that *foxj1* is first expressed in a graded fashion in the LRO anlage at blastula stages, implying that patterning of cilia differentiation in LRO begins early (Blum et al., 2014b). Our results are consistent with this idea since we show that a prepattern evident at blastula stages influences the strain response. For example, cilia lengthening and positioning in response to strain only occurs in a mesodermal, but not an ectodermal context. Explants taken at different dorsal-ventral positions of the marginal zone default to the same short, immotile cilia in the absence of strain, but respond to exogenous strain in a graded manner. Finally, nr2 and foxj1/nr2 explants show a strain response similar to the 90 and 45 degree marginal zone explants, respectively, suggesting that this prepattern likely arises during mesodermal induction, and patterning of *foxj1* expression along the dorsal-ventral axis of the marginal zone. A confounding factor in previous studies in analyzing the formation of this prepattern is that these events also specify the properties of deep mesodermal cells required for gastrulation movements, and thus strain generation. Deep mesodermal cells, positioned under the LRO epithelium, extend the A-P body axis via convergent-extension, using cell behaviors dependent on the PCP pathway, secreted Wnts acting in a permissive manner, and FGF signaling (Heisenberg and Solnica-Krezel, 2008; Keller, 2012; Roszko et al., 2009). Any approach that disrupts these cell behaviors will disrupt axial elongation, reducing strain in the overlying LRO, and indirectly affecting cilia differentiation and the establishment of the A-P planar axis. Thus, a complex interplay between mesodermal patterning, and morphogenesis appear to be required to specify cilia differentiation in the LRO, and this makes the genetic dissection of where key players are likely to directly act challenging. The ability to experimentally separate strain generation from mesodermal patterning in our experiments was essential for dissecting apart these intertwined processes.

Temporal and spatial pattern of ciliation required for left-right patterning

Why is strain used as a cue to reinforce a prepattern that may already be present in the LRO anlage at blastula stages? One possibility is spatial in nature: the LRO anlage undergoes a significant change in shape during gastrulation, resulting in significant amounts of cell mixing that erodes any spatial prepattern. In this light, using the levels of strain as an instructive cue could ensure that cells at the midline are homogenously motile, flanked by LRO cells that are immotile and flow sensors. A second possibility is temporal in nature: cilia formation, lengthening, acquisition of motility, and planar positioning begins in the

Xenopus LRO after gastrulation, but are ongoing processes as L-R patterning occurs, between stage 13 and 18 (Schweickert et al., 2007). In this light, the pattern of high strain in the LRO ensures that critical features required for flow generation begin first and early at the midline, by promoting the formation of a robust A-P planar axis, inducing the formation of motile cilia capable of repositioning along this axis, and promoting a marked increase in cilia length. Thus, mechanical cues may be effective at ensuring the appropriate spatial and temporal sequence of cilia differentiation, best optimized to robustly carry out flow-based patterning given the short developmental window dedicated to this process.

STAR Methods

Contact for Reagent and Resource Sharing

Further information and requests for resources and reagents should be directed to and will be fulfilled by the Lead Contact, Chris Kintner (Kintner@salk.edu).

Experimental Model and Subject Details

Xenopus laevis adults purchased from Nasco were maintained in an aquatic facility at the Salk Institute. *Xenopus e*mbryos were generated using *in vitro* fertilization according to standard protocols, cultured in 0.1X MMR (Sive et al., 1998), and staged according to Nieuwkoop and Faber (1967) (Nieuwkoop and Faber, 1967). Embryos of undetermined sex were used from stages 12 through 18 as indicated. The Salk Institute IACUC approved all animal procedures used in this study, in accordance with AAALAC accreditation.

Method Detail

RNA synthesis and injection—Embryos were typically injected with capped synthetic RNAs at the two-four cell stage, targeting the animal pole or marginal zone as appropriate. RNA transcripts were generated *in vitro* using Sp6 polymerase on CS2-based templates that have been described previously, including *fzd3-GFP, vangl2-GFP, celsr1-GFP, membrane-RFP*, *cep152-GFP,* and *clip170-GFP* (Campbell et al., 2016; Chien et al., 2015). *Tektin2* was identified as a gene strongly upregulated by foxj1 (Stubbs et al., 2008), that was subsequently obtained as Mochii clone Xl.008o07 in pBS, excised using Xho1 and Xba1, and cloned in-frame downstream of GFP using a CS2-based vector. Arl13b-GFP was purchased from Addgene, (Plasmid#40872), and used as template to generate a PCR product that was inserted into CS2 using gateway cloning.

Foxj1 mutants generated using Crispr mutagenesis—A template for generating a gRNA that targets all *foxj1* alleles in *Xenopus laevis* was generated in vitro using PCR (Bhattacharya et al., 2015), based on a targeting sequence described previously (Campbell et al., 2016). The PCR template was column purified and used to generate gRNA using T7 polymerase (Promega) following the manufacture's protocol, and buffer conditions. gRNAs were treated with DNAase1 (RNAase free, Promega), Phenol-Chloroform extracted, and ethanol precipitated, once with ammonium acetate, and then with sodium acetate as the salt. gRNA was resuspended in 15–20 μl DEPC-treated water (typical yield 2.5 μg). Cas9 protein (2.5μl (PNA-Bio #CP01) at 1μg/μl) along with a gRNA (2.5 μl) were allowed to assemble on

ice for 15 mins, and then injected once (1–5 nl) into the animal pole 20–40 minutes after fertilization (Campbell et al., 2016).

Explants and treatment with exogenous strain—All embryonic tissue explants or the LRO were dissected and cultured in Danlichik's for Amy (DFA) (Mitchell et al., 2007). Dorsal marginal zone explants were excised and attached to fibronectin-coated glass (FN explants), held in place by placing a piece of a glass coverslip using silicon grease, as described previously (Davidson et al., 2002). The glass coverslip was removed around stage 12-equivalent to avoid interfering with cilia growth. Keller sandwich explants were generated by placing two giant explants together, initially also held in place by immobilization under a glass coverslip. Animal cap explants were obtained by excising a small central region (approximately 300 μm square) from stage 10.5 embryos that were previously injected with RNAs encoding foxj1, nr2, or the two together. LRO explants were generated by dissecting a small region of the DMZ centered on the dorsal midline and extending approximately 15 degrees around the circumference. Both animal cap and LRO explants were incubated in DFA for 30 minutes for recovery before applying strain, using a microcapillary with inner diameter of 216 μm and a pressure of 50Pa to mimic the strain levels in medial LRO *in situ* or 20Pa to mimic strain levels likely to occur in the more lateral LRO or in ventral ectoderm (Chien et al 2015).

Fluorescence Recovery after Photobleaching (FRAP)—The fraction of stable PCP complexes at the cell junction was measured using the FRAP analysis, as described previously (Chien et al., 2015), using an approach pioneered in *Drosophila* (Strutt et al., 2011). Briefly, RNAs encoding GFP-labeled PCP components were injected into two-four cell embryos, using the minimal level required for imaging, thus avoiding developmental defects. Explants or the LRO were cultured in DFA, and mounted under a glass coverslip for imaging, using a Zeiss LSM 780 or Zeiss AiryScan confocal microscopy. A short junctional segment was selected, bleached using the output of an argon laser (<10%) set to 488, and then images collected at a rate of 1 frame/sec. Ten frames before bleaching were used to establish 100% and the frame at bleaching as set to 0%, after subtracting background fluorescence. The recovery of GFP fluorescence for each PCP component was recorded with Zeiss Zen, and fitted to a one-phase exponential equation (Strutt et al., 2011) in order to define a plateau that could be used to calculate the stable fraction. Full statistics and sample size used in FRAP analysis are presented in Table S1.

Apical Microtubule Orientation—Apical MT orientation was analyzed by live imaging of the LRO or explants expressing the MT-plus end tracer, GFP-tagged clip170 following RNA injection (Chien et al., 2015; Harumoto et al., 2010). The LRO or explants were mounted under a glass coverslip in order to image foci of clip170-GFP located within 1 micron of the apical surface using a Zeiss LSM780 or Zeiss AiryScan confocal microscopy through a 63X lens, recording at the speed of 1s/frame for 1 minute. The movies were then used for measure the angle of each comet within a cell in relation to the A-P body axis or to the axis of applied strain, as well as the direction along these axes. The distribution of the comet angles and direction was represented on a Rose plot as described previously

(Harumoto et al., 2010). Full statistics and sample size used in the analysis of MT orientation are presented in Table S1.

Microtubule standard deviation (MTSD)—The alignment of apical MTs was evaluated by calculating the average deviation of MT orientation from a mean direction of all MTs as described previously (Gomez et al., 2016). The angle between the planar direction of individual MTs at the apical surface in relation to the mean direction was measured manually with ImageJ, using the clip170-GFP comet tracks as the input. The mean angle and the angular standard deviation of the comets inside a cell was calculated using circular statistics (Chien et al., 2015; Gomez et al., 2016).

Cilia motility—Embryos were injected with Arl13b-GFP RNA at the 2-cell stage for cilia live imaging (Boskovski et al., 2013). Explants were isolated at stage 10, strained (or unstrained as a control) for 3 hours at 50Pa, expelled and then cultured until a stage 18 equivalent, all in DFA. Explants were mounted in DFA under a glass coverslip, using minimal pressure to avoid tissue compression. Regions of the explant (typically at the edge) where the cilia were free to move were imaged using a Zeiss Airyscan confocal microscopy with a 63x objective lens and 488 nm argon laser. Images were taken at a speed of 60 ms per frame with proper stacks in Z-direction and processed with Zeiss Zen Airyscan processing function. The cilia beating movie was made from the maximum intensity projection on the Z-stack with around 0.6 to 0.8 second per frame depending on the thickness of the Z-stack. The motility of each cilium was determined by the stillness or circular motion of each cilium in the image sequence. Around 60 cilia were scored for each experiment.

Cilia planar position—Polar plots are used to depict the relative position of a cilium along the planar axis of the apical domain. The location of the centroid of each cell was defined as the origin of the polar plot and the cell boundary as the circumference, normalized to one. The position of the basal body within the plot is determined by both the distance and angle of the dot relative to the origin using ImageJ. Cilia positioning is calculated based on absolute distance in μm from the geometric center, as well as the relative distance defined as the ratio of the distance between the centroid and the cilium, and the distance between the centroid and the cell boundary. Full statistics and sample size used in the analysis of cilia positioning are presented in Table S1.

Length-Width Ratio (LWR)—The cell contours were delineated with β-catenin antibody staining or by injecting embryos at the 2–4cell stage with RNA encoding a membrane RFP. The LWR of each cell was assessed by first defining the long and short axis using a minimum binding box algorithm. Briefly, the apical surface of each cell is treated as a two-dimensional polygon, and the x-y coordinates of the polygon vertices are measured manually with ImageJ. These coordinates are used to calculate a convex hull with the scipy.spatial package ConvexHull function of Python programming language (Jones et al 2001). A rotating calipers algorithm is then used to find the minimum-binding box for the polygon, thus defining the length of a long axis and the corresponding orthogonal axis. Dividing the former by the latter produces a LWR. This approach was also used to determine cell orientation in the embryo or in explants, by defining the orientation of the long axis, as

described above, and plotting this orientation in relation to the A-P body axis, or to the axis of strain. In unstrained explants, cell orientation was plotted in relation to an axis defined as mean direction of cell orientation in that explant.

RNAseq analysis—*Nr2* RNA was injected in the four animal pole quadrants at the 2–4 cell stage, after titering the amounts injected to avoid excessive convergent-extension (~100pg in total/embryo). The animal pole ectoderm was isolated from injected embryos at st10.5 (blastula-stage), and cultured in DFA until stage 14 equivalent. A total of ten explants were pooled and extracted for total RNA, using the proteinase-K approach, followed by phenol/Chloroform extraction, followed by LiCl precipitation. RNA was subjected to polyA selection and then converted into RNAseq libraries, using the Illumina Truseq RNA Sample Preparation kit v2 according to the manufacturer's instructions, and sequenced on a HiSeq 2000 or 2500 at 1×50 or 1×100 base pairs to a depth of 20–40 million reads. Two biological replicates were carried out using Nr2 injected embryos, fertilized, injected and processed on different days. Sequence files used in this analysis can be accessed in GEO under accession numbers GSE76342 and GSE112364.

Bioinformatics—Sequenced reads were quality-tested using FASTQC (Andrew, 2010) and aligned to the *Xenopus laevis* (V9.1) genome using the STAR aligner (Dobin et al., 2013) version 2.4.0k. Mapping was carried out using default parameters (up to 10 mismatches per read, and up to 9 multi-mapping locations per read). The genome index was constructed using the gene annotation provided by the Mayball models. Uniquely mapped reads were quantified across all gene exons using the top-expressed isoform as proxy for gene expression with the HOMER (Heinz et al., 2010) analysis suite, and differential gene expression was carried out with edger (Robinson et al., 2010) using duplicates to compute within-group dispersion. Differentially expressed genes were defined as having a false discovery rate (FDR) <0.05 and a log2 fold change >1 when comparing two experimental conditions. Table S3 reports normalized (counts per 10 million uniquely mapped reads), log2 fold change, and FDR adjusted p-value. Table S3 also reports HOMER functional term overrepresentation of GO biological process, KEGG, Reactome, and Wikipathways with expressed genes corrected for multiple-testing using the Benjamini and Yekutieli general correction for multiple testing (Benjamini and Hockberg, 1995).

Quantification and Statistical Analysis—Full sample size, and statistical analysis of LWR, MT orientation, cilia length, PCP FRAP, Fz3-GFP stability, planar positioning of cilia, and axonemal localization of tektin2-GFP are provided in Table S1, including the standard deviation and p-value based on a student's two-way t-test. Data presented in the text are expressed as the mean±standard deviation, and p-values are calculated based on student's two-tailed t-test. Each experiment was carried out at least twice using multiple embryos or explants. Approach taken to convert cilia length, LWR and planar positioning data into the plots shown in Figures 1, 4, S3 and S5 are provided in Supplemental Statistical methods and Table S2.

Supplementary Material

Refer to Web version on PubMed Central for supplementary material.

Acknowledgments

The authors thank Drs. Jeff Axelrod, Martin Blum, and members of the lab for discussion and suggestions on the manuscript. We also thank Dr. Charles Stevens for suggestions on the quantitative analysis. This work was supported by an NIH grant R01HD092215 to C.K, a Kavli Institute for Brain and Mind grant to S.S., and by the Waitt Advanced Biophotonics Core Facility of the Salk Institute with funding from NIH-NCI CCSG: P30 014195, NINDS Neuroscience Core Grant: NS072031 and the Waitt Foundation.

References

Andrew S. FastQC: a quality control tool for high throughput sequence data. 2010

Antic D, Stubbs JL, Suyama K, Kintner C, Scott MP, Axelrod JD. Planar cell polarity enables posterior localization of nodal cilia and left-right axis determination during mouse and Xenopus embryogenesis. PLoS One. 2010; 5:e8999. [PubMed: 20126399]

Benjamini R, Hockberg Y. Controlling the false discovery rate: a practical and powerful approach to multiple testing. Journal of the Royal Statistical Society. 1995; 57:289–300.

Beyer T, Danilchik M, Thumberger T, Vick P, Tisler M, Schneider I, Bogusch S, Andre P, Ulmer B, Walentek P, et al. Serotonin signaling is required for Wnt-dependent GRP specification and leftward flow in Xenopus. Curr Biol. 2012; 22:33–39. [PubMed: 22177902]

Bhattacharya D, Marfo CA, Li D, Lane M, Khokha MK. CRISPR/Cas9: An inexpensive, efficient loss of function tool to screen human disease genes in Xenopus. Dev Biol. 2015; 408:196–204. [PubMed: 26546975]

Blum M, Feistel K, Thumberger T, Schweickert A. The evolution and conservation of left-right patterning mechanisms. Development. 2014a; 141:1603–1613. [PubMed: 24715452]

Blum M, Schweickert A, Vick P, Wright CV, Danilchik MV. Symmetry breakage in the vertebrate embryo: when does it happen and how does it work? Dev Biol. 2014b; 393:109–123. [PubMed: 24972089]

Borovina A, Superina S, Voskas D, Ciruna B. Vangl2 directs the posterior tilting and asymmetric localization of motile primary cilia. Nature cell biology. 2010; 12:407–412. [PubMed: 20305649]

Boskovski MT, Yuan S, Pedersen NB, Goth CK, Makova S, Clausen H, Brueckner M, Khokha MK. The heterotaxy gene GALNT11 glycosylates Notch to orchestrate cilia type and laterality. Nature. 2013; 504:456–459. [PubMed: 24226769]

Campbell EP, Quigley IK, Kintner C. Foxn4 promotes gene expression required for the formation of multiple motile cilia. Development. 2016; 143:4654–4664. [PubMed: 27864379]

Chien YH, Keller R, Kintner C, Shook DR. Mechanical Strain Determines the Axis of Planar Polarity in Ciliated Epithelia. Curr Biol. 2015; 25:2774–2784. [PubMed: 26441348]

Choksi SP, Lauter G, Swoboda P, Roy S. Switching on cilia: transcriptional networks regulating ciliogenesis. Development. 2014; 141:1427–1441. [PubMed: 24644260]

Chu CW, Ossipova O, Ioannou A, Sokol SY. Prickle3 synergizes with Wtip to regulate basal body organization and cilia growth. Scientific reports. 2016; 6:24104. [PubMed: 27062996]

Chu CW, Sokol SY. Wnt proteins can direct planar cell polarity in vertebrate ectoderm. eLife. 2016:5.

Davidson LA, Hoffstrom BG, Keller R, DeSimone DW. Mesendoderm extension and mantle closure in Xenopus laevis gastrulation: combined roles for integrin alpha(5)beta(1), fibronectin, and tissue geometry. Dev Biol. 2002; 242:109–129. [PubMed: 11820810]

Davidson LA, Keller R, DeSimone D. Patterning and tissue movements in a novel explant preparation of the marginal zone of Xenopus laevis. Gene Expr Patterns. 2004; 4:457–466. [PubMed: 15183313]

Dobin A, Davis CA, Schlesinger F, Drenkow J, Zaleski C, Jha S, Batut P, Chaisson M, Gingeras TR. STAR: ultrafast universal RNA-seq aligner. Bioinformatics. 2013; 29:15–21. [PubMed: 23104886]

Gomez JM, Chumakova L, Bulgakova NA, Brown NH. Microtubule organization is determined by the shape of epithelial cells. Nat Commun. 2016; 7:13172. [PubMed: 27779189]

Hamada H, Tam PP. Mechanisms of left-right asymmetry and patterning: driver, mediator and responder. F1000prime reports. 2014; 6:110. [PubMed: 25580264]

Harumoto T, Ito M, Shimada Y, Kobayashi TJ, Ueda HR, Lu B, Uemura T. Atypical cadherins Dachsous and Fat control dynamics of noncentrosomal microtubules in planar cell polarity. Dev Cell. 2010; 19:389–401. [PubMed: 20817616]

Hashimoto M, Hamada H. Translation of anterior-posterior polarity into left-right polarity in the mouse embryo. Curr Opin Genet Dev. 2010; 20:433–437. [PubMed: 20439159]

Hashimoto M, Shinohara K, Wang J, Ikeuchi S, Yoshiba S, Meno C, Nonaka S, Takada S, Hatta K, Wynshaw-Boris A, et al. Planar polarization of node cells determines the rotational axis of node cilia. Nature cell biology. 2010; 12:170–176. [PubMed: 20098415]

Heinz S, Benner C, Spann N, Bertolino E, Lin YC, Laslo P, Cheng JX, Murre C, Singh H, Glass CK. Simple combinations of lineage-determining transcription factors prime cis-regulatory elements required for macrophage and B cell identities. Mol Cell. 2010; 38:576–589. [PubMed: 20513432]

Heisenberg CP, Solnica-Krezel L. Back and forth between cell fate specification and movement during vertebrate gastrulation. Curr Opin Genet Dev. 2008; 18:311–316. [PubMed: 18721878]

Hellman NE, Liu Y, Merkel E, Austin C, Le Corre S, Beier DR, Sun Z, Sharma N, Yoder BK, Drummond IA. The zebrafish foxj1a transcription factor regulates cilia function in response to injury and epithelial stretch. Proc Natl Acad Sci U S A. 2010; 107:18499–18504. [PubMed: 20937855]

Keller R. Developmental biology. Physical biology returns to morphogenesis. Science. 2012; 338:201–203. [PubMed: 23066066]

Keller R, Jansa S. Xenopus Gastrulation without a blastocoel roof. Dev Dyn. 1992; 195:162–176. [PubMed: 1301081]

Keller RE. Vital dye mapping of the gastrula and neurula of Xenopus laevis. I. Prospective areas and morphogenetic movements of the superficial layer. Dev Biol. 1975; 42:222–241. [PubMed: 46836]

Keller RE. Vital dye mapping of the gastrula and neurula of Xenopus laevis. II. Prospective areas and morphogenetic movements of the deep layer. Dev Biol. 1976; 51:118–137. [PubMed: 950072]

LeGoff L, Lecuit T. Mechanical Forces and Growth in Animal Tissues. Cold Spring Harb Perspect Biol. 2015; 8:a019232. [PubMed: 26261279]

Matis M, Russler-Germain DA, Hu Q, Tomlin CJ, Axelrod JD. Microtubules provide directional information for core PCP function. eLife. 2014; 3:e02893. [PubMed: 25124458]

McGrath J, Somlo S, Makova S, Tian X, Brueckner M. Two populations of node monocilia initiate left-right asymmetry in the mouse. Cell. 2003; 114:61–73. [PubMed: 12859898]

Minegishi K, Hashimoto M, Ajima R, Takaoka K, Shinohara K, Ikawa Y, Nishimura H, McMahon AP, Willert K, Okada Y, et al. A Wnt5 Activity Asymmetry and Intercellular Signaling via PCP Proteins Polarize Node Cells for Left-Right Symmetry Breaking. Dev Cell. 2017; 40:439–452. e434. [PubMed: 28292423]

Mitchell B, Jacobs R, Li J, Chien S, Kintner C. A positive feedback mechanism governs the polarity and motion of motile cilia. Nature. 2007; 447:97–101. [PubMed: 17450123]

Neugebauer JM, Amack JD, Peterson AG, Bisgrove BW, Yost HJ. FGF signalling during embryo development regulates cilia length in diverse epithelia. Nature. 2009; 458:651–654. [PubMed: 19242413]

Nieuwkoop, PD., Faber, J. Normal table of *Xenopus Laevis*. Amersterdam: North Holland; 1967.

Nonaka S, Yoshiba S, Watanabe D, Ikeuchi S, Goto T, Marshall WF, Hamada H. De novo formation of left-right asymmetry by posterior tilt of nodal cilia. PLoS biology. 2005; 3:e268. [PubMed: 16035921]

Okada Y, Takeda S, Tanaka Y, Izpisua Belmonte JC, Hirokawa N. Mechanism of nodal flow: a conserved symmetry breaking event in left-right axis determination. Cell. 2005; 121:633–644. [PubMed: 15907475]

Quigley IK, Kintner C. Rfx2 Stabilizes Foxj1 Binding at Chromatin Loops to Enable Multiciliated Cell Gene Expression. PLoS Genet. 2017; 13:e1006538. [PubMed: 28103240]

Quigley IK, Stubbs JL, Kintner C. Specification of ion transport cells in the Xenopus larval skin. Development. 2011; 138:705–714. [PubMed: 21266406]

Robinson MD, McCarthy DJ, Smyth GK. edgeR: a Bioconductor package for differential expression analysis of digital gene expression data. Bioinformatics. 2010; 26:139–140. [PubMed: 19910308]

Roszko I, Sawada A, Solnica-Krezel L. Regulation of convergence and extension movements during vertebrate gastrulation by the Wnt/PCP pathway. Semin Cell Dev Biol. 2009; 20:986–997. [PubMed: 19761865]

Schier AF. Nodal signaling in vertebrate development. Annu Rev Cell Dev Biol. 2003; 19:589–621. [PubMed: 14570583]

Schweickert A, Vick P, Getwan M, Weber T, Schneider I, Eberhardt M, Beyer T, Pachur A, Blum M. The nodal inhibitor Coco is a critical target of leftward flow in Xenopus. Curr Biol. 2010; 20:738–743. [PubMed: 20381352]

Schweickert A, Weber T, Beyer T, Vick P, Bogusch S, Feistel K, Blum M. Cilia-driven leftward flow determines laterality in Xenopus. Curr Biol. 2007; 17:60–66. [PubMed: 17208188]

Shih J, Keller R. Patterns of cell motility in the organizer and dorsal mesoderm of Xenopus laevis. Development. 1992; 116:915–930. [PubMed: 1295744]

Shimada Y, Yonemura S, Ohkura H, Strutt D, Uemura T. Polarized transport of Frizzled along the planar microtubule arrays in Drosophila wing epithelium. Dev Cell. 2006; 10:209–222. [PubMed: 16459300]

Shook DR, Majer C, Keller R. Pattern and morphogenesis of presumptive superficial mesoderm in two closely related species, Xenopus laevis and Xenopus tropicalis. Dev Biol. 2004; 270:163–185. [PubMed: 15136148]

Sive, H., Grainger, RM., Harland, RM. The early development of Xenopus laevis: a laboratory manual. Plainview, NY: Cold Spring Harbor Press; 1998.

Song H, Hu J, Chen W, Elliott G, Andre P, Gao B, Yang Y. Planar cell polarity breaks bilateral symmetry by controlling ciliary positioning. Nature. 2010; 466:378–382. [PubMed: 20562861]

Strutt H, Warrington SJ, Strutt D. Dynamics of core planar polarity protein turnover and stable assembly into discrete membrane subdomains. Dev Cell. 2011; 20:511–525. [PubMed: 21497763]

Stubbs JL, Oishi I, Izpisua Belmonte JC, Kintner C. The forkhead protein Foxj1 specifies node-like cilia in Xenopus and zebrafish embryos. Nat Genet. 2008; 40:1454–1460. [PubMed: 19011629]

Tozser J, Earwood R, Kato A, Brown J, Tanaka K, Didier R, Megraw TL, Blum M, Kato Y. TGF-beta Signaling Regulates the Differentiation of Motile Cilia. Cell reports. 2015; 11:1000–1007. [PubMed: 25959824]

Tuft PH. The uptake and distribution of water in the embryo of Xenopus laevis (Daudin). The Journal of experimental biology. 1962; 39:1–19. [PubMed: 13923033]

Walentek P, Beyer T, Thumberger T, Schweickert A, Blum M. ATP4a is required for Wnt-dependent Foxj1 expression and leftward flow in Xenopus left-right development. Cell reports. 2012; 1:516–527. [PubMed: 22832275]

Walentek P, Schneider I, Schweickert A, Blum M. Wnt11b is involved in cilia-mediated symmetry breakage during Xenopus left-right development. PLoS One. 2013; 8:e73646. [PubMed: 24058481]

Yoshiba S, Hamada H. Roles of cilia, fluid flow, and Ca2+ signaling in breaking of left-right symmetry. Trends Genet. 2014; 30:10–17. [PubMed: 24091059]

Yoshiba S, Shiratori H, Kuo IY, Kawasumi A, Shinohara K, Nonaka S, Asai Y, Sasaki G, Belo JA, Sasaki H, et al. Cilia at the node of mouse embryos sense fluid flow for left-right determination via Pkd2. Science. 2012; 338:226–231. [PubMed: 22983710]

Highlights

1. Different ciliated cells in the left-right organizer (LRO) produce and sense fluid flow
2. Mechanical strain in the *Xenopus* LRO specifies flow producing ciliated cells
3. Mechanical strain also specifies a global planar axis required for leftward flow
4. Strain is a developmental cue linking cilia planar positioning and motile differentiation

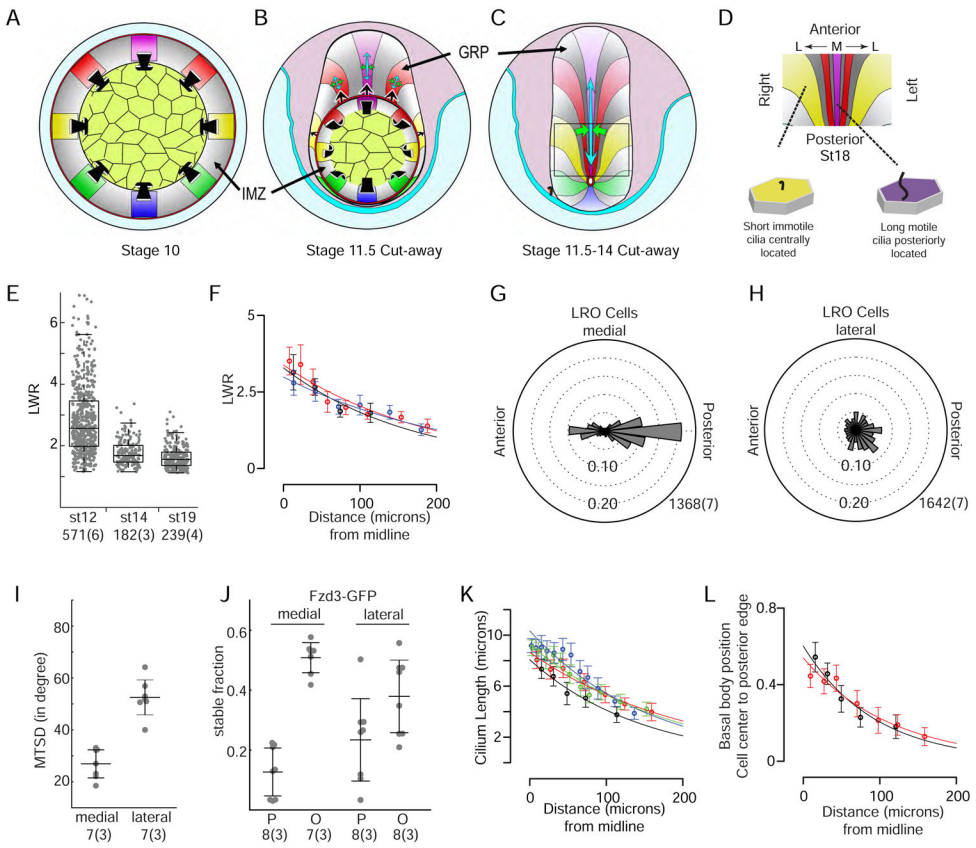

Figure 1. Strain, polarized microtubules and PCP components in the LRO

(A–C) Diagrams of the vegetal (A) and dorsoposterior aspects (B, C) of the *Xenopus* embryo during gastrulation illustrate the development of patterns of strain in the IMZ, and the presumptive GRP, during gastrulation. See text for explanation. **(D)** After gastrulation, the LRO (boxed area in C, inverted and viewed from the inside) differentiates by forming flow producing cells medially (M. long motile cilia that reposition to the posterior cell edge), and flow sensing cells laterally (immotile short cilia that remain in a more central planar position). **(E)** The LWR of LRO cells at different stages are shown on a Tukey box plot. **(F)** The LWR of cells in three LROs at stage 12 is plotted versus position along the M-L axis, combining data from both sides, showing the average for equivalent size bins, the 95% confidence range, and the best-fit curve (Table S2). **(G–H)** Polar plots summarizing MT orientation in medial (G) and lateral (H) LRO cells (Fig. S2A–B, Table S1). **(I)** MT alignment within medial and lateral LRO cells, where each point represents the standard deviation from the mean for an individual cell (Table S1). **(J)** Plots summarizing the stable fraction of fz3-GFP at junctions oriented parallel (P) or orthogonal (O) to the A-P axis, in medial and lateral LRO cells (Table S1). **(K–L)** Cilia length (K) and planar positioning (L) are plotted versus cell position in the LRO at stage 18, as the average for equivalent size bins, the 95% confidence range, and the best-fit curve (Table S2). Planar positioning is measured as a distance from the geometric center (0) to the posterior cell edge (1) normalized to one. Full statistics and sample size for these data are provided in Table S1.

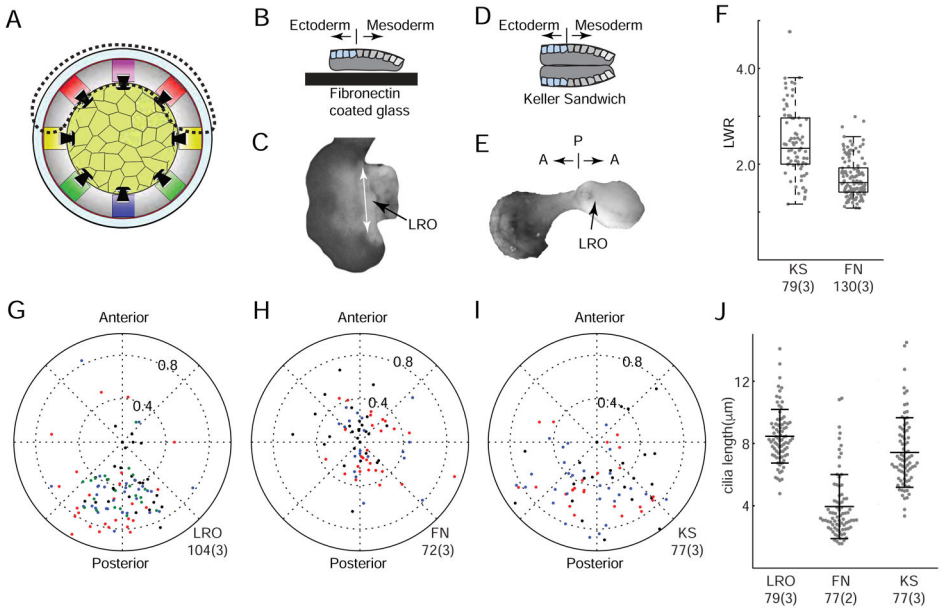

Figure 2. Ciliation defects in explants that lack strain

(A–E) Dorsal explants (dotted line, A) cultured on fibronectin (FN explants,B) or placed together into a Keller sandwich (KS explants, D). Axial elongation is suppressed in FN explants (C, top view) but rescued KS explants (E, top view). **(F)** LWR of LRO cells at a stage 12 equivalent in FN and KS explants summarized on a Tukey box plot. **(G–I)** Basal body position in LRO cells *in situ* (G), or in a FN (H) or KS explant (I) at a stage 18-equivalent, plotted in relation to the geometric cell center (center) and the cell edge normalized to one. Plots are aligned to the A-P axis as indicated in KS explant (E) or FN explant (white line, C). Data from different embryos or explants are color-coded. **(J)** Plots of cilia length at the midline of the explants or the LRO (mean±s.d.). Full statistics and sample sizes are provided in Table S1.

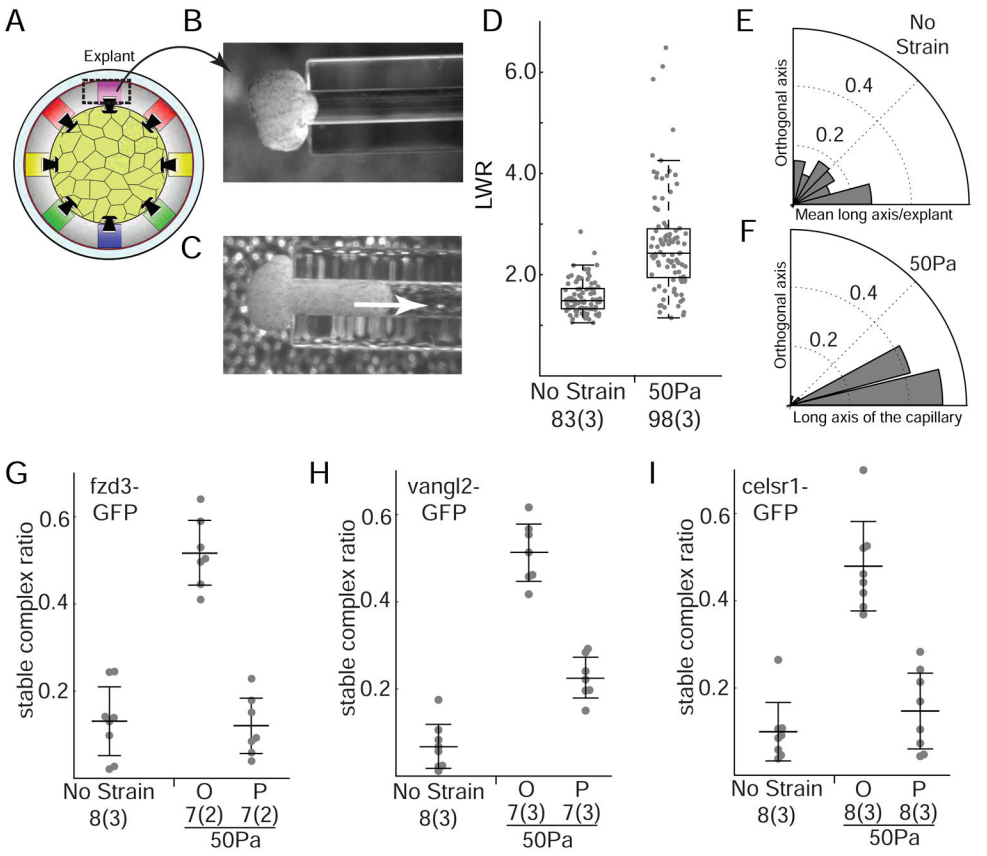

Figure 3. Strain promotes planar axis formation in LRO explants

(A–F) LRO explants isolated as indicated (A) were left unstrained (B) or gradually strained (C) by aspiration into a capillary (50 Pa, 3hrs). At a stage 12 equivalent, cell elongation (LWR) and orientation was scored and shown on a Tukey plot (D), or rose plot (E–F), respectively. The number of cells (explants) scored is indicated. Rose plots indicate the fraction of cells scored that align to the X-axis (set to the long axis of the capillary in strained explants or to mean long axis in unstrained explants), versus orthogonal, y-axis. **(G–I)** The stable fraction of fzd3-GFP (G), vangl2-GFP (H), and celsr1-GFP (I) was measured using FRAP, at junctions in the LRO explants at a stage 12-equivalent, either unstrained or after 3 hrs of aspiration (50Pa). Junctions measured in unstrained explants were randomly chosen, while those in strained explants were chosen based on whether they lie parallel (P) or orthogonal (O) to the strain axis. Error bars show the mean±s.d.. Full statistics and sample size are presented in Table S1.

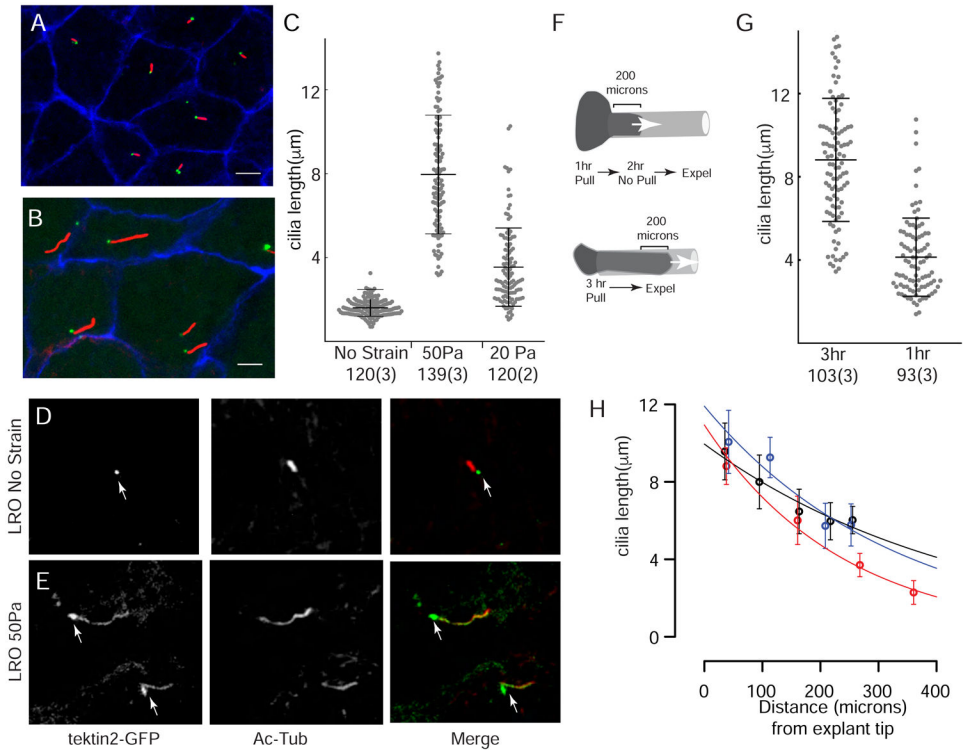

Figure 4. Strain promotes long motile cilia formation in LRO explants

(A–B) Confocal images of LRO explants at a stage 18-equivalent, either left unstrained (A) or strained for 3hrs using 50Pa of negative pressure (B), visualizing cell boundaries (blue), basal bodies (green) and cilia (red). **(C)** Cilia length at a stage 18 equivalent in LRO explants either left unstrained, or strained for 3 hours using relatively high (50Pa) or low (20Pa) levels of negative pressure. **(D–E)** Confocal images of representative cilia in strained (E) and unstrained LRO explants, expressing tektin2-GFP, and stained with the acetylated tubulin antibody. Arrows mark basal body location of tektin2-GFP. **(F–G)** Diagrams (F) illustrating two different strain applications that vary in strain duration (3 versus 1 hour), following by cilia length measurements (G) at a stage 18 equivalent. **(H)** Cilia length at a stage 18-equivalent in LRO explants that were strained for 3 hours with 50Pa. Shown are plots of data from individual explants where cilia length is plotted versus cell position in the explant during strain, showing the average for equivalent size bins, the 95% confidence range, and the best-fit curve (Table S2). Full statistics and sample size are provided in Table S1.

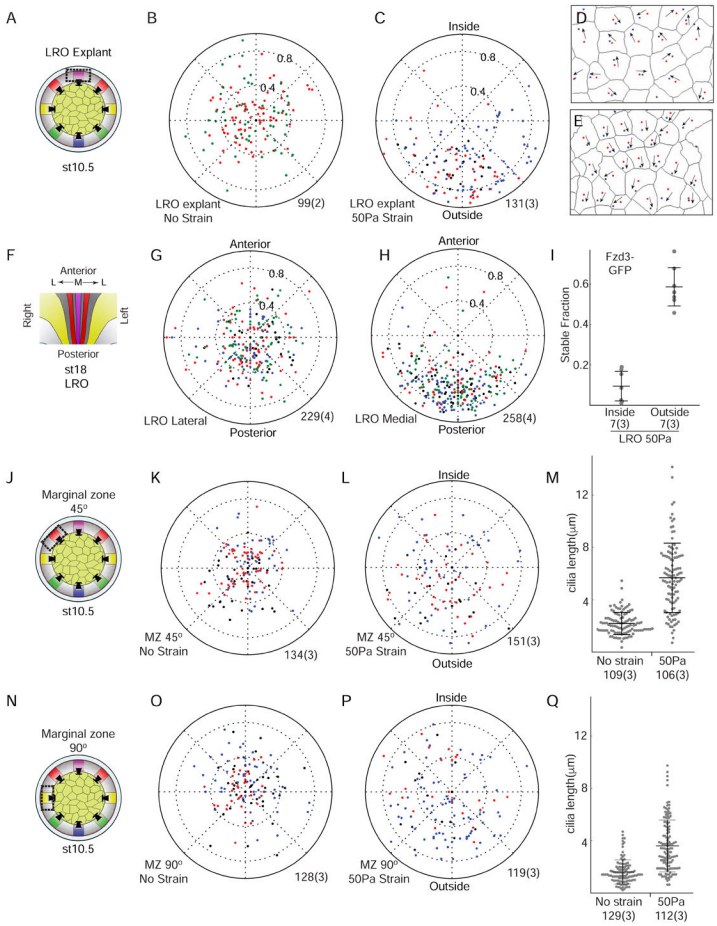

Figure 5. Strain induces cilia positioning and a PCP vector in a consistent planar direction

(A–E) LRO explants (A) were left unstrained (B,D) or strained for 3hrs using 50 Pa of negative pressure (C,E). Basal body position plotted as in Figure 2 with different colors used in these and other panels to represent data from different explants. Plots are oriented along the inside-to-outside axis of the capillary in the strained explants, but randomly assigned in the unstrained explants. Examples of basal body positioning data from unstrained (D) and strained explants (E), where the red dot is the geometric center, the blue dot is the basal body, black is the cell edges, and the arrows denote the planar vector. **(F–H)** Planar positioning of cilia in the LRO in situ (F) shown in polar plots as above, based on data obtained for lateral (G) versus medial cells (H). **(G)** FRAP analysis of isolated, *Fzd3-GFP* expressing LRO cells at a stage 12 equivalent. Inside and outside refer to cell edges furthest and closest to opening of the capillary, respectively. **(J–Q)** Marginal zone explants, centered either 45 degrees (J–M) or 90 degrees (N–Q) from the dorsal midline, were left unstrained (K,O) or strained (L,P) using the same conditions employed for LRO explants. At a stage-18 equivalent, cilia length (M,Q) and planar positioning (K–L, O–P) were scored and plotted, as above. Full sample size and statistics are presented in Table S1.

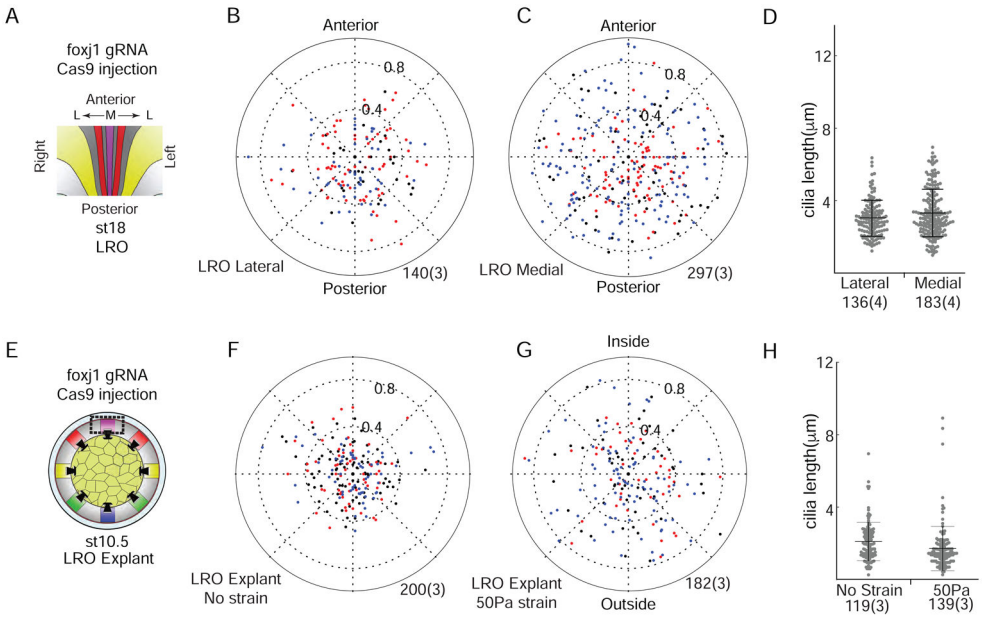

Figure 6. Foxj1 is required for strain-induced cilia differentiation

(A–D) Cilia length (D) and planar position (B,C) was measured in the LRO of *foxj1* Crispr mutants at stage 18 (A), in cells located laterally (B) or medially (C). **(E–H)** Cilia length (H) and planar position (F,G) were measured at a stage 18 equivalent in LRO explants isolated from *foxj1* mutants (E) and left unstrained (F) or subjected to strain (G) for 3hrs using 50Pa of negative pressure. Full statistics and sample sizes are provided in Table S1.

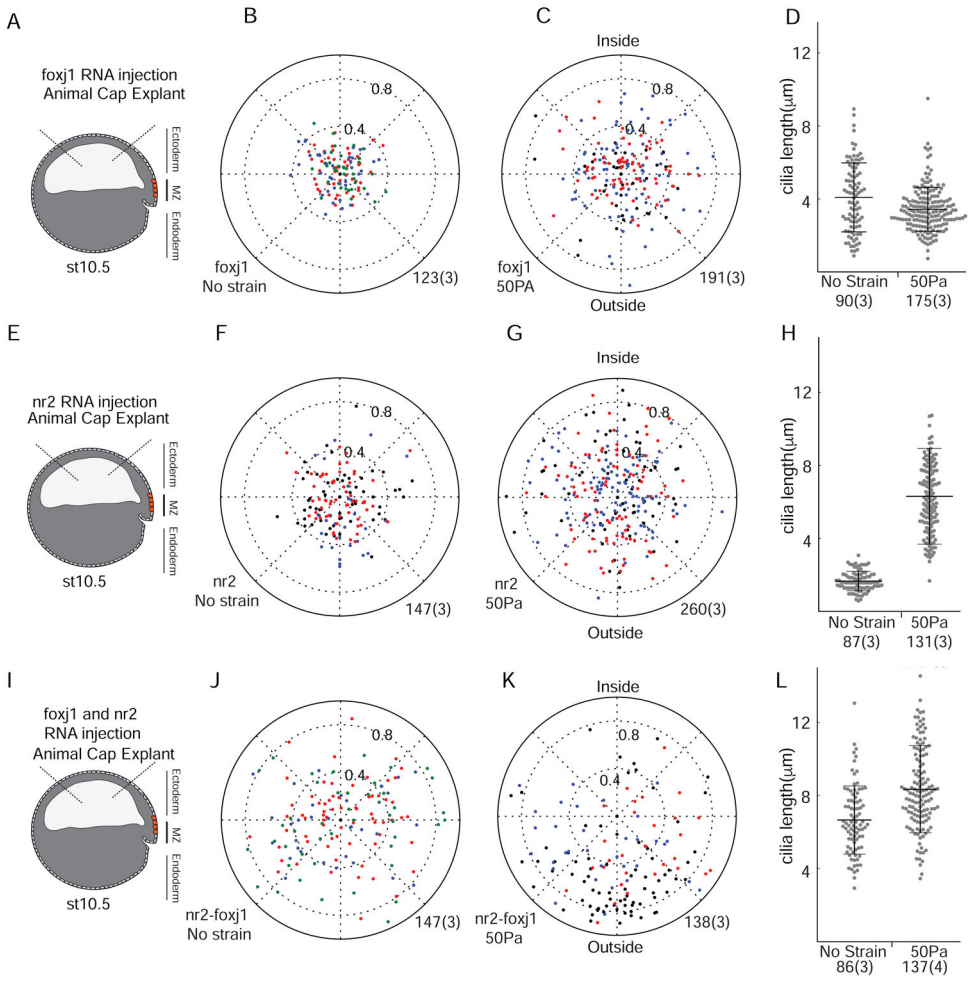

Figure 7. Deconstructing cilia differentiation in response to strain

(A–L) Ectodermal explants expressing foxj1 (A–D), nr2 (E–H) or both foxj1/nr2 (I–L) were left unstrained (B,F,J) or strained for 3hrs using 50Pa of negative pressure (C,G,K). At a stage 18 equivalent, cilia length (D,H,L) and planar positioning (B,C,F,G,J,K) were scored as described in Figure 5. The axes in panels B, F and J were assigned randomly for each individual explant, with data from a given explant color-coded. Polar plots in panels C, G and K are oriented relative to the inside and outside of the capillary during strain. Full statistics and sample sizes are provided in Table S1.